Journal of Chromatography A, 1217 (2010) 6230–6240

Contents lists available at ScienceDirect

Journal of Chromatography A

journal homepage: www.elsevier.com/locate/chroma

A novel approach to modelling counter-current chromatography

Hacer Guzlek[a,b,*], Ines I.R. Baptista[a], Philip L. Wood[b], Andrew Livingston[a]

[a] Imperial College London, South Kensington Campus, London SW7 2AZ, UK
[b] Dynamic Extractions Ltd., 890 Plymouth Road, Slough, Berkshire SL1 4LP, UK

ARTICLE INFO

Article history:
Received 1 June 2010
Received in revised form 2 August 2010
Accepted 5 August 2010
Available online 11 August 2010

Keywords:
Counter-current chromatography
CCC
Liquid–liquid chromatography
Modelling
Elution profile prediction
Continuous-stirred tank reactor
CSTR
Mass balance
gPROMS

ABSTRACT

Literature lists a number of counter-current chromatography (CCC) models that can predict the retention time and to a certain extent the peak width of a solute eluting from a CCC column. The approach described in this paper distinguishes itself from previous reports by relating all model parameters directly to column dimensions and experimental settings. Most importantly, this model can predict a chromatogram from scratch without resorting to traditional calibration using empirical values. The model validation with experimental results obtained across a range of CCC instruments demonstrated that the solute retention time, peak width, and peak resolution could be predicted within reasonable accuracy. Additionally, the effect of several process parameters, such as mobile phase flow rate, rotational speed of the column or β-value, showed that the model is robust and applicable to a wide range of CCC instruments. Overall, this model proved to be a useful tool for parameter estimation and, most significantly, separation optimisation.

1. Introduction

Counter-current chromatography (CCC) is a liquid–liquid chromatography technique that separates components of a mixture based on their distribution between two immiscible liquid phases. One of these phases is used as the mobile phase the other one as the stationary phase [1,2]. Solutes elute from the CCC column according to their partition ratio (K_D), which is defined as the ratio of the solute's concentration in the stationary phase to its concentration in the mobile phase [3]. Compounds, which have a higher affinity to the mobile phase (low K_D), elute earlier, while compounds that have a higher affinity to the stationary phase (high K_D) elute later. In CCC the retention of a solute in the column is directly proportional to its partition ratio and thus it is mathematically predictable. Using the classical solute retention equation (Eq. (1)) the retention volume of the peak maximum can be predicted [3]:

$$t_R = \frac{V_C}{F}[S_f(K_D - 1) + 1] \quad (1)$$

The column is first filled with the stationary phase and rotated. After reaching the set rotational speed, mobile phase is pumped into the column at the selected flow rate. Due to the density difference between mobile and stationary phases, the mobile phase will travel towards the column outlet displacing a certain amount of stationary phase and eventually elute from the column. When no more stationary phase is displaced, the column has reached hydrodynamic equilibrium. The stationary phase retention S_f is the relative amount of stationary phase in comparison to the column volume at hydrodynamic equilibrium. Wood et al. [4] derived an equation to predict the stationary phase retention of solvent combinations.

The CCC column is generally made of a length of tubing wound around a bobbin. In J-type coil-planet-centrifuges, the bobbin is mounted on a planetary axis, which is driven by a central axis [5]. Thus, the column rotates around its own axis as well as around a central axis creating a cardioid motion. The centrifugal force created by the column rotation facilitates retaining the liquid stationary phase inside the column while the mobile phase is pumped through the column. The rotation of the column generates a force field. The ratio of centripetal acceleration at the rotor radius to that of the gravity at the Earth's surface at sea level ($g = 9.81\ \mathrm{m\,s^{-2}}$) is termed as the g-level. The g-level at the centre of the column of a CCC instrument is calculated as in Eq. (2):

$$g\text{-level} = \frac{R\omega^2}{9.81} \quad (2)$$

* Corresponding author at: Dynamic Extractions Ltd., 890 Plymouth Road, Slough, Berkshire SL1 4LP, UK. Tel.: +44 175 369 69 79; fax: +44 175 369 69 76.
E-mail addresses: Hguzlek@imperial.ac.uk, hacer.guzlek@dynamicextractions.com (H. Guzlek).

0021-9673/$ – see front matter.
doi:10.1016/j.chroma.2010.08.011

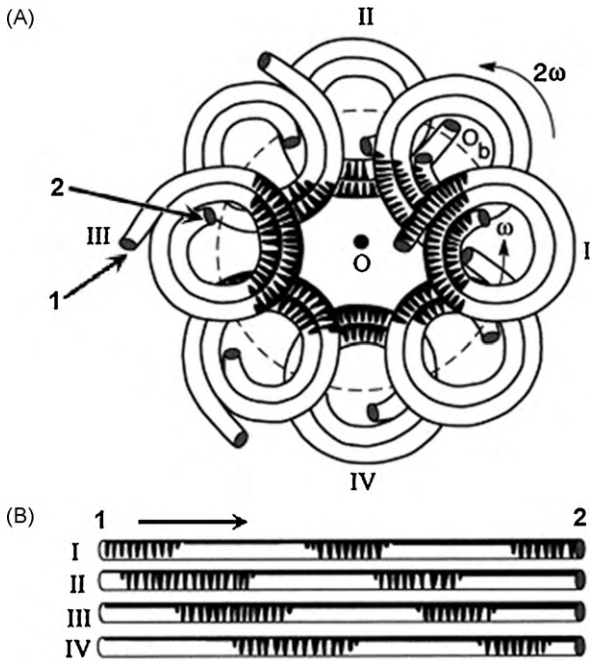

Fig. 1. (A) Schematic demonstration of the mixing zones' motion inside a multilayer column, where 1 and 2 indicate the inlet and outlet of the column; O is the central axis, O_b is the orbital axis; (B) mixing zone travels from 1 to 2 as displayed in positions I, II, II, and IV in an unwound column.
Adapted from Ref. [5]

The cardioid motion generates a series of sequential mixing and settling zones along the length of the column. When the column is operating, every loop of tubing around the bobbin contains a mixing zone (region of loop closest to the central axis) and a settling zone (region of loop farthest from the central axis), see Fig. 1(A) [6]. With every full rotation of the column a mixing zone moves forward one loop in the column. In Fig. 1(B) the column is presented as unwound tubing and areas of mixing are localised in rotational positions I, II, III, and IV; it is shown that the mixing wave always moves in one direction depending on the column rotation [6].

Conway [3] reported that the instantaneous volume ratio between mixing and settling zones is determined by the β-value. The β-value is the ratio of planet radius (r) to the orbital radius (R) (see Eq. (3)):

$$\beta = \frac{r}{R} \tag{3}$$

The angle of the sector where the mixing starts and ends can be calculated using Eq. (4) (as in Fig. 2):

$$\sin \gamma_r^* = \cos \Theta^* = -\frac{R}{4r} = -\frac{1}{4\beta} \tag{4}$$

A number of CCC modelling papers can be found in the literature. One modelling concept suggested using a discrete staged-cell model to describe axial dispersion and a continuous diffusion model to represent longitudinal mixing [7]. It was known that when the rate of longitudinal mixing was low, which is the case when column length L to diameter d ratio is greater than hundred ($L/d > 100$), the discrete and continuous models gave the same results [8–10]. Kostanian [7] considered the cell model and started off using a mass balance equation for an individual cell assuming reaching perfect equilibrium. However, the equation was not further handled as a differential equation, but transformed to represent residence time distributions in a chromatographic column. The cell model approach described was conceptually strong, but mathematically simply handled. Given readily available computing power and choice in mathematical modelling tools, the mass balance equation could have been solved as a differential equation to determine the elution profile.

Another significant approach reported in the literature was adapting the counter-current distribution theory [11]. In this model, the CCC column was modelled using an array of positions representing a chain of test tubes in one dimension and mixing, settling, and transfer activities in the other. The model was further extended to simulate other operation modes such as co-current and dual flow CCC [12]. It was validated successfully in analytical as well as production scales and proved to yield accurate results for peak retentions; however, peak widths were not predicted precisely. A major drawback of this model was that the number of test tubes in the series was empirically calibrated or estimated to give the "best fit" to an existing chromatogram and not correlated to instrument parameters.

The models in the literature can predict solute retention and to a certain extent peak resolution. However, they require empirical calibration and do not take instrument parameters into account. The aim of this work was to overcome this existing limitation by implementing a model that can calculate a chromatogram from scratch based on instrument parameters.

2. Theory

The CCC column is modelled based on mass balance equations in a series of identical continuous-stirred tank reactors (CSTRs)

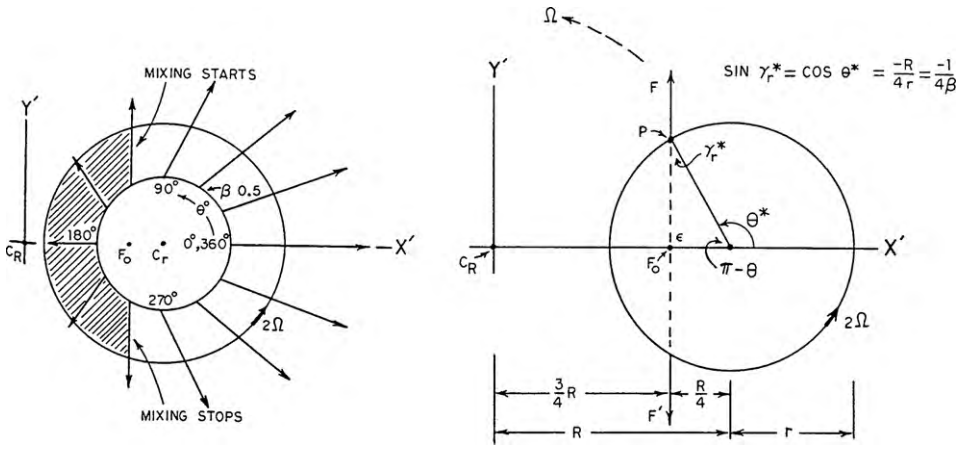

Fig. 2. Mixing start and end positions in a CCC column are determined by the angle Θ or γ_r^*; are dependent on the β-value and can be calculated using Eq. (4) [3].

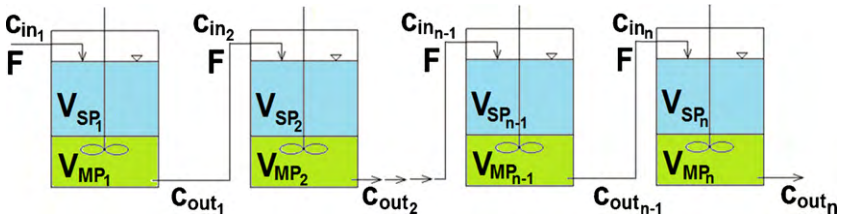

Fig. 3. Series of n identical CSTRs containing two liquid phases, solute is injected into the first CSTR ($n = 1$), from second reactor on ($n \geq 2$), the outlet of the previous becomes inlet of the next CSTR ($c_{out,n-1} = c_{in,n}$).

containing two immiscible liquid phases. Therefore the following assumptions were made.

In CCC the velocity of a mixing wave (v_{mix}) is considerably higher than the mobile phase velocity (v_{MP}), because a mixing wave moves forward the length of one column loop with every column rotation and typical rotational speeds are several hundreds to thousands per minute; whereas a mobile phase increment usually precedes only a limited number of loops per minute. This means by the time a mobile phase increment has moved forward the entire length of the mixing area, it has experienced tens to hundreds of mixing and settling cycles. The mobile phase increment is assumed to be the length of one mixing wave and this segment is assumed to be fully equilibrated. Hence, the entire length of the column is taken as a series of fully equilibrated CSTRs.

The $v_{mix} : v_{MP}$ ratio determines how many mixing and settling zones a mobile phase segment experiences. The minimum value for this ratio, which is required for a solute concentration in the mobile phase segment to reach perfect equilibrium, is not known. If it was known, this would mean that below this value either the mobile phase proceeds too quickly with respect to the mixing zone velocity or the mixing zone velocity is too slow for the given flow rate. However, there is a limit for both at which no stationary phase would be retained inside the column and a separation would not take place. Hence, another model assumption is that as long as stationary phase is retained in the column, the behaviour of a solute concentration in the column can be represented by the CSTR model. In the CSTR model the rotational speed of the column affects the stationary phase retention, but does not directly influence separation efficiency when using low to medium viscosity solvents. For high viscosity solvents column modifications could be required to retain stationary phase in the column. In such cases the model assumptions need to be adjusted according to these column parameters.

The number of CSTRs is directly proportional to the number of instantaneous mixing zones. It is determined by the number of column loops.

In Section 1 it was stated that the volume of a mixing zone in a multilayer column depends on the loop size and β-value, hence mixing zone volumes in outer loops are larger than in inner loops. In order to simplify the model, the volume of every mixing zone was considered equal.

The CSTRs have identical volumes and are filled with stationary and mobile phases while respecting the stationary phase retention for a given solvent system in the CCC column (see Fig. 3). The mobile phase flow rate F, stationary and mobile phase volumes V_{SP} and V_{MP}, the solute concentration c_{in}, and its partition ratio K_D are known. The pulse (injection) is introduced into the first CSTR in the series; from the second tank onwards the outlet concentration of the previous CSTR ($c_{out,n-1}$) is the inlet concentration of the next ($c_{in,n}$).

The stationary phase remains in each CSTR, whereas the mobile phase is continuously washed through according to the mobile phase flow rate. The solute enters the mixing zone, distributes between the two phases as per partition ratio and leaves this zone successively with the mobile phase. Ideal mixing and instantaneous distribution of the solute between the two phases are assumed. The mass balance in the individual CSTRs over time is described as:

$$V_{MP}\frac{dc_{MP,n}}{dt} + V_{SP}\frac{dc_{SP,n}}{dt} = F \times c_{in,n} - F \times c_{MP,n} \quad (5a)$$

Because K_D is the concentration of the solute in the stationary phase divided by its concentration in the mobile phase, Eq. (5a) can be transformed into Eq. (5b):

$$V_{MP}\frac{dc_{MP,n}}{dt} + V_{SP} \times K_D\frac{dc_{MP,n}}{dt} = F \times c_{in,n} - F \times c_{MP,n} \quad (5b)$$

where the volume of the mobile and stationary phases in each CSTR can be calculated according to Eq. (6):

$$V_{\mathrm{CSTR}} = V_{SP} + V_{MP} = \frac{V_{SP}}{S_f} \quad (6)$$

Since instantaneous mixing is assumed, the solute concentration in the mobile phase in a CSTR is also the outlet concentration from this CSTR. Hence, the mobile phase concentration in the last CSTR represents the outlet concentration from the CCC column.

The CSTR volume, V_{CSTR}, is calculated using Eq. (4), rotor radius R, average bobbin radius r_B, average β-value, β_B, and internal diameter d_c of the column, and length of the mixing zone L_{CSTR}:

$$V_{\mathrm{CSTR}} = \left(\frac{d_c}{2}\right)^2 \pi L_{\mathrm{CSTR}} \quad (7)$$

$$L_{\mathrm{CSTR}} = \frac{r_B \pi \alpha}{180} \quad (8)$$

$$\alpha = 2\ \cos^{-1}\left(\frac{R}{4r_B}\right) = 2\cos^{-1}\left(\frac{1}{4\beta_B}\right) \quad (9)$$

The loop volume V_{Loop} is calculated similarly:

$$V_{Loop} = \left(\frac{d_c}{2}\right)^2 \pi L_{Loop} \quad (10)$$

$$L_{Loop} = 2\pi r_B \quad (11)$$

The next step is to calculate the V_{Loop} to V_{CSTR} ratio in order to determine how many consecutive CSTRs there are in one loop. This ratio is then multiplied with the number of loops n_{Loop} in a column to determine the number of CSTRs (n_{CSTRs}) for a given column:

$$n_{\mathrm{CSTRs}} = n_{Loops}\frac{V_{Loop}}{V_{\mathrm{CSTR}}} \quad \therefore \quad n_{\mathrm{CSTRs}} = n_{Loops}\frac{(d_c/2)^2\pi r_B 2\pi}{(d_c/2)^2\pi((r_B\pi 2\cos^{-1}(1/4\beta_B))/180)} \quad \therefore \quad n_{\mathrm{CSTRs}} = n_{Loops}\frac{180}{\cos^{-1}(1/4\beta_B)} \quad (12)$$

Some parameters cancel out and ultimately, Eq. (12) indicates that the number of CSTRs depends on the number of column loops and the average β-value. It is worth mentioning that this equation represents the approximate number of CSTRs to simplify the model. In order to calculate the exact values, loop volumes and respective V_{CSTR} must be individually calculated for every layer of tubing, which then have to be simulated individually.

The gPROMS CSTR model consists of two individual models; the oneCSTR model and a Connector model (see Fig. 4). The oneCSTR

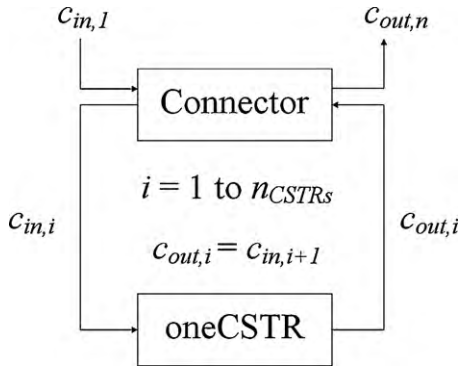

Fig. 4. Model diagram, the CSTR model consists of two model entities, the Connector and the oneCSTR models; the oneCSTR model contains the mass balance equation of one CSTR; the Connector supplies the inlet concentration and obtains the outlet concentration and creates a loop of inlet and outlet streams for every individual CSTR in the series of n_{CSTRs}; these streams are indexed with i where i is an increment between 1 and n_{CSTRs}; the concentration introduced into the column is c_{in}, this is used by the Connector to create the first inlet stream $c_{in,i}$; the oneCSTR model calculates the $c_{out,i}$ concentration, which is used as $c_{in,i+1}$ for the next CSTR in the series by the Connector model.

model contains the mass balance equation, which calculates the outlet concentration c_{out} for a given inlet concentration c_{in} of a CSTR. The Connector model consists of a loop of n inlet and outlet streams for every individual CSTR in the series; where i is an increment between 1 and n. It supplies the oneCSTR model with the inlet concentration $c_{in,i}$ and obtains the outlet concentration $c_{out,i}$, which is then fed back into the oneCSTR model as $c_{in,i+1}$. The first inlet concentration $c_{in,1}$ for the first CSTR in the series is the concentration introduced into the column c_{in}. The loop is then repeated until the outlet concentrations for all CSTRs are calculated. This means in the course of a simulation the inlet and outlet concentrations of all CSTRs and therefore the entire length of the column can be monitored.

The initial and boundary conditions are given in Eqs. (13)–(15):

$$c_{in}(t_0) = 0 \tag{13}$$

$$c_{out}(t_0) = 0 \tag{14}$$

$$c_{in}(t) = \begin{cases} c_{in}(t) & t < t_{inj}(\text{injection}) \\ 0 & t_E \leq t\,(\text{elution}) \end{cases} \tag{15}$$

The first inlet variable c_{in} can be reset after a certain time, i.e. zero if injection starts straight away or after a certain time to include extra column volume between the sample loop and the column. In order to include the extra column volume, the time it takes for the sample to reach the column can be calculated by dividing the extra column volume by the flow rate. The inlet concentration is reset to zero after the injection time (t_{inj}), which is sample loop volume divided by the mobile phase flow rate. After resetting the inlet concentration the model runs for the set elution time t_E.

Using the CSTR model, the elution profile of a solute can be calculated as concentration leaving the column over a selected time period. As the most common detection method is UV/VIS absorption, chromatograms can be normalised if required (see Section 3).

3. Materials and methods

3.1. gPROMS

The model equation system was developed and solved using gPROMS v3.2.0 (Process Systems Enterprise Ltd, London, UK). gPROMS (general PROcess Modelling System) is an advanced equation-oriented process modelling software by Process Systems Enterprise Ltd. It solves a system of algebraic equations, partial differential equations, integral equation or mixed systems of these types of equations using fast and robust numerical solution techniques [19]. For all simulations a tolerance of 10^{-5} was used. All simulations were performed on a 2.4 GHz Intel Core Duo CPU with 4 GB RAM.

3.2. Counter-current chromatography

3.2.1. Apparatus

Experimental CCC results reported in literature were used for the model validation. These results were obtained using a range of CCC instruments from Dynamic Extractions (DE, Slough, UK) and two prototype instruments by Sandlin and Ito [15]. The specifications for these instruments are presented in Table 1. The angle of the mixing zone segment was calculated using Eq. (4) and the average arc length of the mixing zone was determined. This was used to calculate the average mixing zone volume. Then, the number of CSTRs was calculated using Eq. (12).

3.2.2. Experiments for validation

The ratio of the mixing zone velocity v_{mix} ($\mathrm{m\,s^{-1}}$) and the mobile phase velocity v_{MP} ($\mathrm{m\,s^{-1}}$) as in Table 2 was calculated using Eqs. (16) and (17):

$$v_{mix} = L_{Loop} \times \text{rotational speed} \tag{16}$$

$$v_{MP} = \frac{F}{\pi(d_c/2)^2(1 - S_f)} \tag{17}$$

The GUESS solute mixture is a combination of readily available standards with varying polarities and was first reported by Friesen and Pauli [13]. The GUESS mixture as used in this publication contained red new coccine, caffeine, nicotinic acid, ferulic acid, umbelliferone, aspirin, and vanillin. Guzlek et al. [14] used this mixture to evaluate the effect of rotational speed and mobile phase flow rate on the resolution of a CCC separation. These results were taken into consideration for the model validation. The injection conditions, 5 mg of each compound was injected in 4 mL of the biphasic solvent system, were also used for the simulations [14]. Further operational and experimental details that were used for model validations can be found in Tables 2 and 3.

The effect of β-value was validated using experimental results obtained by Sandlin and Ito [15]. For the development of large-scale preparative counter-current chromatographic machines Sandlin and Ito investigated the effect of increasing the diameter of the column. The resulting β-values and other column parameters for these columns can be found in Table 1. The experimental data was plotted in a spreadsheet and overlaid with the theoretical results. Since the same compounds, detector and flow rate were used and the compounds had very similar molar absorbance, the modelling results could be normalised by determining the absorption factor, which was 7 for all shown comparisons in Section 4.3.

In order to validate different CCC instrument types, scale-up results by Wood et al. [16] and Sutherland et al. [17] were selected. In this case a separation carried out using a 0.0054 L column volume instrument was scaled up directly to two pilot scale instruments with 4.6 and 18 L column volume each. Sutherland et al. used a mixture of benzyl alcohol and p-cresol for this scale up.

3.2.3. Absorbance normalisation

All experimental separations were monitored with a UV/vis detector. Depending on the flow cell in a detector, the signal strength varied among detectors. Hence, in order to align the ordinate (y-axis) scales of simulated and experimental results, a normalisation factor was necessary. Therefore the signal output in absorbance was normalised by dividing the experimental

Table 1
Specification for a series of CCC instruments used for model validation.

Instrument type	Rotor radius (mm)	Number of spools	Column bore (mm)	Column length (m)	Column volume (mL)	Number of loops	Typical rotational speed	β-value range	Number of CSTRs
DE Mini	50	1	0.8	35.8	18	200	2100	0.50–0.76	540
DE Millie	50	1	0.8	35.8	5.4	51.5	2100	0.50–0.76	132
DE Spectrum	85	2	1.6	67.6	136	190	1600	0.52–0.86	497
DE Midi	110	2	4	72.6	912	168	1400	0.51–0.88	346
DE Maxi	300	2	10	58.6	4600	40	600	0.70–0.84	101
DE New Maxi	300	2	10	229.2	18000	168	600	0.53–0.92	433
Sandlin & Ito 1	150	1	5.5	30	750	61[a]	300	0.50–0.55	177[a]
Sandlin & Ito 2	150	1	5.5	30	750	116[a]	300	0.25–0.30	846[a]

[a] These are approximate values as the numbers of loops for these columns were not mentioned; hence they were determined dividing the column length by the average column loop radius, which was calculated considering the average column radius from the β-value.

Table 2
Operational parameters of separation experiments used for model validation, F is flow rate, v_{mix} is the velocity of mixing wave ($m\,s^{-1}$), v_{MP} is the mobile phase velocity ($m\,s^{-1}$), S_f is the stationary phase retention.

Separation	Instrument	F ($mL\,min^{-1}$)	Ratio v_{mix} : v_{MP}	S_f (%)	Extra column volume (mL)	V_{sample} (mL)	Absorption factor
GUESS 240g – A	DE Spectrum	1.5	24	88	2	4	3 500 000
GUESS 240g – B	DE Spectrum	3.0	30	85	2	4	3 500 000
GUESS 240g – C	DE Spectrum	6.0	51	74	2	4	3 500 000
GUESS 80g – A	DE Spectrum	1.5	26	77	2	4	3 500 000
GUESS 80g – B	DE Spectrum	3.0	41	64	2	4	3 500 000
GUESS 80g – C	DE Spectrum	6.0	53	53	2	4	3 500 000
Sandlin & Ito A	Ito & Sandlin 1	8.3	149	65	Not mentioned	20	7
Sandlin & Ito B	Ito & Sandlin 1	8.3	47	79	Not mentioned	20	7
Sandlin & Ito C	Ito & Sandlin 2	8.3	68	84	Not mentioned	20	7
Sandlin & Ito D	Ito & Sandlin 2	8.3	29	87	Not mentioned	20	7
Wood et al. A	DE Millie	1	88	64	0.94	1.07	6.9
Wood et al. B	DE Maxi	850	45	47	483	920	6.4
Sutherland et al.	DE New Maxi	850	27/55[a]	66/31[a]	Not mentioned	1 100	0.3

[a] It was reported that the stationary phase retention was 66% after reaching the hydrodynamic equilibrium, however further stationary was displaced in the course of the experiment; 31% stationary phase was left in the column at the end of the separation.

values by the absorption factor for chromatograms generated by a detector. The absorption factor was determined by overlaying the experimental and simulation results and dividing the highest experimental y-axis value by the highest simulation y-axis value.

3.2.4. Individual and additive simulation profiles

The described gPROMS model calculates the elution profile of individual solutes separately. These results (concentrations) can be added up (additive simulation results) in a similar fashion as the signal output of a detector. With that a better comparison of simulated and experimental resolutions can be obtained.

3.2.5. Resolution error calculation

Resolutions were calculated using Eq. (18), where t_{ra} and t_{rb} are the retention times at the peak maxima and W_a and W_b are the respective peak widths:

$$R_s = \frac{2(t_{ra} - t_{rb})}{W_a + W_b} \tag{18}$$

The error (in %) for resolutions was calculated by dividing the absolute difference between experimental and simulation resolutions by the experimental resolution.

3.3. Integration of areas

In a correct model it would be expected that the peak area corresponds to the injected mass. Integration of peak areas gave the same value (accuracy of four decimal places was considered) as the introduced pulse. The equations were solved numerically, hence the accuracy of the peak integration was provided

Table 3
Solvent systems and partition ratios K_D of compounds used for model validation.

Compound	Solvent system (v/v)	Mobile phase	Instrument	K_D	$Mass_{sample}$ (mg)
Red new coccine	Hexane/ethyl acetate/methanol/water, 2/3/2/3	Lower phase	DE Spectrum	0.00	5
Caffeine and Nicotinic acid	Hexane/ethyl acetate/methanol/water, 2/3/2/3	Lower phase	DE Spectrum	0.27	5+5
Ferulic acid	Hexane/ethyl acetate/methanol/water, 2/3/2/3	Lower phase	DE Spectrum	0.74	5
Umbelliferone	Hexane/ethyl acetate/methanol/water, 2/3/2/3	Lower phase	DE Spectrum	1.03	5
Aspirin and Vanillin	Hexane/ethyl acetate/methanol/water, 2/3/2/3	Lower phase	DE Spectrum	1.24	5+5
DNP-ala	Chloroform/acetic acid/0.1N hydrochloric acid, 2/2/1	Lower phase	Ito&Sandlin 1&2	2.00[a]	500
DNP-ala	Chloroform/acetic acid/0.1N hydrochloric acid, 2/2/1	Upper phase	Ito&Sandlin 1&2	1.92[a]	500
DNP-glu	Chloroform/acetic acid/0.1N hydrochloric acid, 2/2/1	Lower phase	Ito&Sandlin 1&2	0.50[a]	500
DNP-glu	Chloroform/acetic acid/0.1N hydrochloric acid, 2/2/1	Upper phase	Ito&Sandlin 1&2	0.42[a]	500
Benzyl alcohol	Heptane/ethyl acetate/methanol/water, 1.4:0.1:0.5:1.0	Lower phase	DE Mini	0.62[a]	45
p-Cresol	Heptane/ethyl acetate/methanol/water, 1.4:0.1:0.5:1.0	Lower phase	DE Mini	1.43[a]	21.4
Benzyl alcohol	Heptane/ethyl acetate/methanol/water, 1.4:0.1:0.5:1.0	Lower phase	DE Maxi	0.85[a]	38 600
p-Cresol	Heptane/ethyl acetate/methanol/water, 1.4:0.1:0.5:1.0	Lower phase	DE Maxi	1.60[a]	18 400
Benzyl alcohol	Heptane/ethyl acetate/methanol/water, 1.4:0.1:0.5:1.0	Lower phase	DE New maxi	0.60[a]	46 200
p-Cresol	Heptane/ethyl acetate/methanol/water, 1.4:0.1:0.5:1.0	Lower phase	DE New maxi	0.86[a]	22 000

[a] Partition ratio determined from CCC chromatogram considering stationary phase retention.

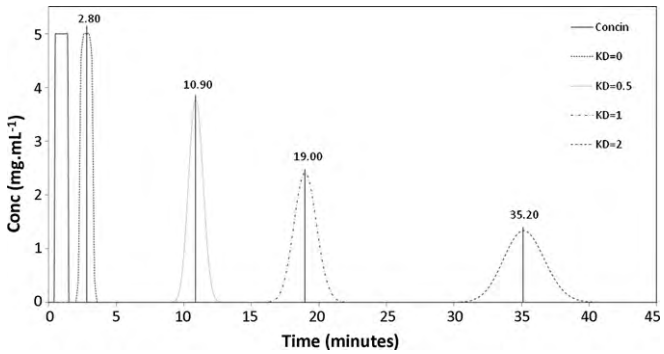

Fig. 5. Solid trace is the introduced pulse: concentration was 5 mg mL^{-1}; injection took place between 0.5 and 1.5 min; dashed or dotted traces are elution profiles of four solutes with partition ratios 0, 0.5, 1, and 2 (simulated retention times at peak maxima is noted in the graph); column volume was 18 mL, stationary phase retention was 90%, mobile phase flow rate was 1 mL min^{-1}, number of CSTRs in series was 540; solutes (concentration 5 mg mL^{-1} each) were injected between 0.5 and 1.5 min of simulation start.

by choosing small steps between calculation intervals (typically 0.2 min).

4. Results and discussion

4.1. Solute retention time

The initial validation of the model was carried out to verify if solutes with different partition ratios eluted according to Eq. (1). Therefore a simulation of four solutes with partition ratios 0, 0.5, 1, and 2 was carried out using the parameters of a DE Mini instrument and the following operational parameters were chosen: 18 mL column volume, 90% stationary phase retention, 1 mL min^{-1} mobile phase flow rate, 0.5 mL extra column volume between injection and column, and 540 CSTRs in the series (calculated by Eq. (12)). The introduced pulse contained 5 mg mL^{-1} of each compound and the injection volume was 1 mL (pulse profile: see solid trace in Fig. 5).

The retention times of solutes in Fig. 5 were compared with retention times calculated using Eq. (15) (see Fig. 6). There was a strong correlation between the residence times; the systematic difference of 0.5 min was due to the sample injection time of 1 min in the CSTR model. In this case the residence time of peaks were related to the centre (peak maximum) of the injected pulse (which in this case is 0.5 min). Eq. (1) does not take injected sample volume into consideration; therefore the solutes were assumed to be introduced and eluted from the column as an infinitely high, sharp pulse with $t_{inj} = 0$.

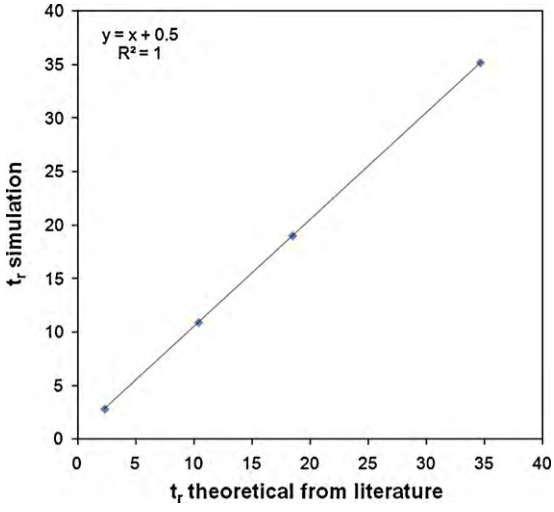

Fig. 6. Comparison of theoretical solute retention times $t_{r,t}$ calculated using Eq. (1) [3] and $t_{r,s}$ from simulation using the CSTR model.

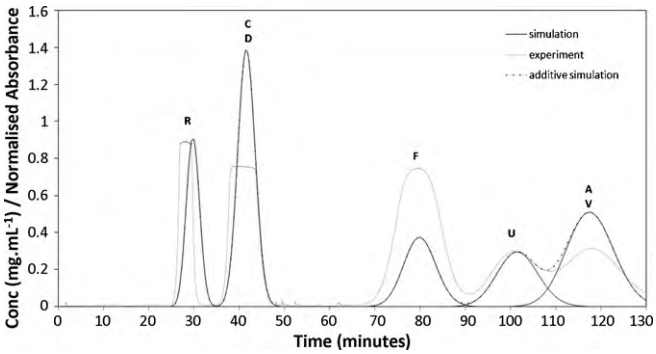

Fig. 7. GUESS 80*g* – A, overlay of experimental (dotted trace – adapted from Ref. [14]), individual simulation (solid trace) and additive simulation (dash-dot trace) results, flow rate was 1.5 mL min^{-1}, 77% stationary phase retention, 497 CSTRs in the model series; compounds red new coccine R, caffeine C, nicotinic acid D, ferulic acid F, umbelliferone U, aspirin A, and vanillin V.

The CSTR model accurately predicted solute retention times, when column parameters, mobile phase flow rate, stationary phase retention in the column, and the solute's mass and partition ratio were known.

4.2. Effect of mobile phase flow rate and rotational speed

The model was further validated using experimental results from literature [14] where a CCC separation of a mixture with seven components using different flow rates and rotational speeds was reported. Operational parameters of these separations were considered in the CSTR model validation. The number of CSTR was calculated as described in Section 2 and was 497 for these experiments. In Figs. 7–12 the overlay of experimental and simulation results can be found. The experimental results were normalised as described in Section 3.2.3.

Solute retention times and peak resolutions of experimental and simulated results were compared. Predicting the resolution was the major challenge for the CSTR model. Previously reported models could not predict peak widths and resolutions from scratch and had to be calibrated using experimental results. It is valuable to predict resolutions, since the resolution determines the purity of a fraction collected over time when carrying out a separation. If the resolution of a separation can be determined accurately, other operational parameters of the separation can be optimised easily

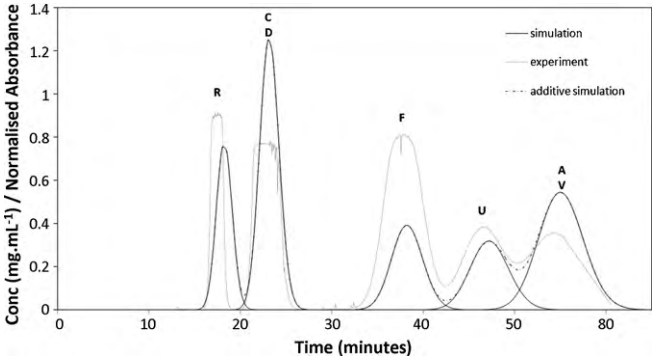

Fig. 8. GUESS 80*g* – B, overlay of experimental (dotted trace—adapted from Ref. [14]), individual simulation (solid trace) and additive simulation (dash-dot trace) results, flow rate was 3 mL min^{-1}, 64% stationary phase retention, 497 CSTRs in the model series; compounds red new coccine R, caffeine C, nicotinic acid D, ferulic acid F, umbelliferone U, aspirin A, and vanillin V.

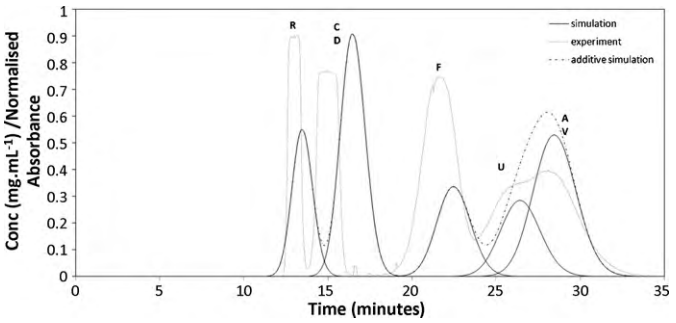

Fig. 9. GUESS 80*g* – C, overlay of experimental (dotted trace—adapted from [14]), individual simulation (solid trace) and additive simulation (dash-dot trace) results, flow rate was 6 mL min^{-1}, 63% stationary phase retention, 497 CSTRs in the model series; compounds red new coccine R, caffeine C, nicotinic acid D, ferulic acid F, umbelliferone U, aspirin A, and vanillin V.

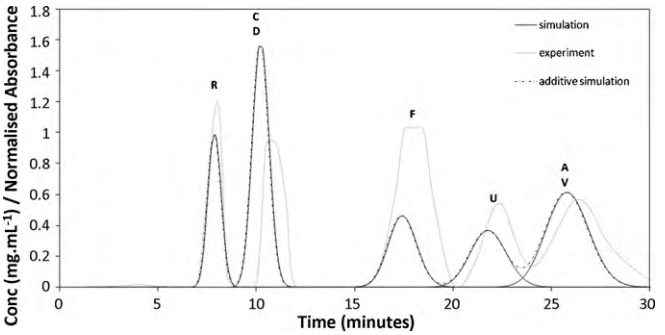

Fig. 12. GUESS 240*g* – C, overlay of experimental (dotted trace—adapted from Ref. [14]), individual simulation (solid trace) and additive simulation (dash-dot trace) results, flow rate was 6 mL min^{-1}, 74% stationary phase retention, 497 CSTRs in the model series; compounds red new coccine R, caffeine C, nicotinic acid D, ferulic acid F, umbelliferone U, aspirin A, and vanillin V.

using the model. This can save time and material when optimising a CCC separation.

In Figs. 7–9 the overlaid experimental and model results (for individual and additive results) of the 80*g* separations are presented. The solute retention times were predicted accurately and peak widths are very similar. The peak heights vary due to distinct absorbance of solutes; the first two experimental peaks (R and C&D peaks) do not resemble a peak as the detector flow cell was saturated and the peak shape was truncated. Ferulic acid (peak F) has a very high molar absorption; thus the experimental peak is significantly higher than the theoretical peak. The simulation results demonstrate peak shapes according to the concentration and hence mass of the eluting solute. Table 4 shows experimental resolutions for peaks F and U, and U and A&V from Ref. [14] and simulated resolutions for respective chromatograms. The comparison of later eluting peaks is particularly important, because the error for peak retention as well as peak width will be larger the higher the partition ratio of a solute is. The experimental resolutions for the GUESS 80*g* – A separation were 1.06 for F and U, and 0.55 for U and A&V, whereas simulated resolutions were 1.13 and 0.67, respectively. This means the errors were 6.6% for F and U, and 21.8% for U and A&V. The average resolution error for the 80*g* separations was 12.4%. It is understood that the experimental detector output is a value for absorbance; therefore if two consecutive peaks overlap, the detector responds by summing the absorbances of both solutes. The model output is a concentration and hence, simulates and displays the elution profile of each solute individually. This means the model displays the elution profile of solutes quantitatively. Therefore, experimental peak resolutions of closely eluting compounds will be smaller than those of simulated peaks. However, the elution profiles of solutes can be added up to give a cumulative elution profile.

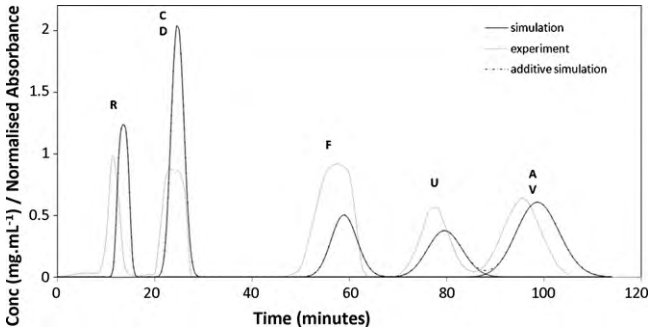

Fig. 10. GUESS 240*g* – A, overlay of experimental (dotted trace—adapted from [14]), individual simulation (solid trace) and additive simulation (dash-dot trace) results, flow rate was 1.5 mL min^{-1}, 88% stationary phase retention, 497 CSTRs in the model series; compounds red new coccine R, caffeine C, nicotinic acid D, ferulic acid F, umbelliferone U, aspirin A, and vanillin V.

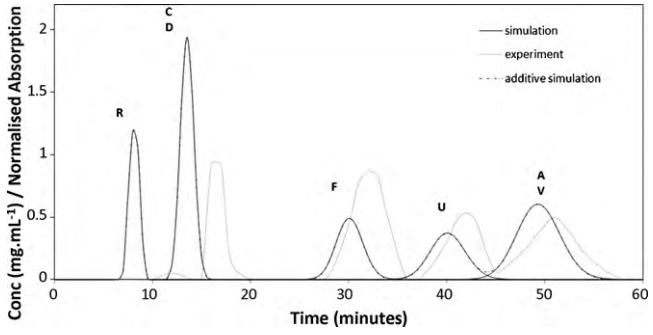

Fig. 11. GUESS 240*g* – B, overlay of experimental (dotted trace – adapted from Ref. [14]), individual simulation (solid trace) and additive simulation (dash-dot trace) results, flow rate was 3 mL min^{-1}, 85% stationary phase retention, 497 CSTRs in the model series; compounds red new coccine R, caffeine C, nicotinic acid D, ferulic acid F, umbelliferone U, aspirin A, and vanillin V.

The overlay of experimental and simulated results of the GUESS 80*g* – B separation is shown in Fig. 8. The peak retention times and widths were accurately predicted. Here again it becomes apparent that the experimental and simulation resolutions vary due to the nature of traces, which were recorded as total absorbance and individual elution profiles. The comparison of experimental and simulation resolutions gave a similar error as the previous (GUESS 80*g* – A) overlay (see Table 4).

The last result set of the 80*g* separations is shown in Fig. 9. In this case the simulated retention times and peak widths of the R and C&D peak differed slightly from the experimental results. The effect of UV detection can be seen very clearly in this example: in the simulation results the peaks of U and A,V can be distinguished clearly, whereas the experimental peaks of these two solutes almost merge to give one peak and resolutions cannot be determined.

Figs. 10–12 present experimental results carried out at 240*g* overlaid with model results using respective operational parameters. Retention times of solutes for these separations were predicted relatively accurately. Also peak shapes of experimental and theoretically calculated peaks look very similar. In Fig. 11 in the experimental trace, the red new coccine peak is missing; the small peak between 10 and 12 min indicates the solvent front and this is where this compound would have eluted.

The peak resolutions were simulated relatively accurately for the 240*g* separations; the largest discrepancy was for the 6 mL min^{-1} separation between F and U with an error of 12.50%. Here it has to be noted that the experimental results exhibit an unusual trend; the resolution was expected to decrease with

Table 4
Comparison of peak resolutions from experimental results from Ref. [14] and from theoretical results using the CSTR model.

Mobile phase flow rate (mL min^{-1})	g-force (m s^{-2})	Experimental resolution (F and U) from Ref. [14]	Simulation resolution (F and U)	Error (%)	Experimental resolution (U and AV) from Ref. [14]	Simulation resolution (U and AV)	Error (%)
1.5	80	1.06	1.13	6.6	0.55	0.67	21.8
3	80	0.97	0.99	2.1	0.58	0.69	19.0
6	80	n.a.	0.89	–	n.a.	0.41	–
1.5	240	1.84	1.84	0.0	1.27	1.21	4.7
3	240	1.60	1.58	1.2	1.14	1.12	1.7
6	240	1.60	1.40	12.5	1.04	1.02	1.9

increasing flow rate as it is the case for the 1.5 mL min^{-1} and 3 mL min^{-1}. However, the resolution between F and U peaks remains the same when increasing the flow rate from 3 mL min^{-1} to 6 mL min^{-1}. The theoretical results decrease in an expected manner for these flow rates; therefore the values for resolution for F and U at 6 mL min^{-1} gave the largest error. The resolutions between U and A&V peaks were very similar even though there was a larger error expected for resolutions of later eluting peaks. Despite the largest error of 12.50%, the overall average error was only 3.69% for all 240*g* separations. This error was much smaller than the average error obtained for the 80*g* separations. This is very likely to be due to the overall improved peak resolutions at 240*g*. As mentioned above, in a UV chromatogram, absorbances of two overlapping solutes add up, whereas individually separated peaks give a chromatogram that is directly proportional to the single solutes concentration eluting from the column (as indicated by the Lambert-Beer rule).

4.3. Effect of β-value

Sandlin and Ito [15] have investigated the effect of the β-value on a separation with the aim of developing large-scale preparative CCC columns. A 0.55 cm I.D. tubing was coiled around two holders with 7.5 and 15 cm diameter to obtain different β-value columns, which had the same volume. The rotor diameter was 30 cm, hence the resulting β-values of these columns varied between 0.25–0.30 and 0.50–0.55. For the evaluation of these columns they used a mixture of dinitrophenyl aminoacids and separated them using the same rotational speed (300 rpm) and mobile phase flow rate (500 mL/h). They demonstrated that the resolutions were significantly higher on the low β-value column. The CSTR model complies with this finding, because if the same length of tubing is wound around a smaller diameter holder, the column will have a higher number of loops. Also the angle γ_r^*, which determines the start and end of the mixing area in the column, is larger the smaller the β-value is. This means the mixing zone volume is smaller the lower the β-value is. Hence in two equal volume columns with different β-values the column with a smaller β-value will have a larger number of CSTRs with smaller mixing zone volumes. This will affect the resolution so that the lower β-value column will show sharper peaks and the resolution will be higher. Another supporting argument that proves the CSTR model to be valid is the $v_{mix} : v_{MP}$ ratio. In the early CCC apparatus, the rotational speeds were relatively low, but this was compensated by using these columns at low flow rates, which resulted in long separation times. Sandlin and Ito used a low rotational speed and kept the mobile phase flow rate relatively low. With that the $v_{mix} : v_{MP}$ ratios were 223 for the low β-value column and 425 for the other one.

The number of loops was not mentioned in Ref. [15], so it was estimated by considering the average wound radius. This was used to determine the average perimeter of one loop, which was then used to divide the column to obtain an approximate number of column loops. From the total length of the column, which was 30 m, the number of loops was computed and was 116 for β-value 0.25–0.30 and 61 for 0.50–0.55. Furthermore, the numbers of CSTRs were calculated using Eq. (12) and were 847 and 177, respectively.

For the simulation the average partition ratios were determined from CCC chromatograms and was 0.42 for DNP-glu and 1.92 for DNP-ala when upper phase was mobile phase and 0.50 DNP-ala for and 2.00 DNP-glu when lower phase was mobile phase.

The experimental and theoretical chromatograms were very similar for the high β-value results (see Figs. 11 and 13). The peak widths of the low β-value simulated results differed slightly from the experimental results (see Figs. 10 and 12)—especially for the later eluting peak. This is very likely to be due to the high number of CSTRs in the series, which results in sharper peaks and increased resolution. The numbers of loops of these columns were not known and hence calculated using the column length and the average column holder diameter. The error is very likely to be larger for the smaller holder. More accurate peak widths for the low β-value column could potentially be obtained if the actual number of loops were known. Despite an estimated value for column loops, the CSTR model accurately predicted the elution profile for different β-value instruments. These examples demonstrate that the CSTR model can be used for instrument parameter optimisation.

Another important note here is that the $v_{mix} : v_{MP}$ ratio did not affect the resolutions. Despite a larger $v_{mix} : v_{MP}$ ratio of the high β-value column, the resolution in this column did not improve. This means that above a certain value for the $v_{mix} : v_{MP}$ ratio, the number of mixing and settling zones that a column segment experiences does not improve resolution. The resolution is mainly determined by the size and number of the mixing zones and thus by the β-value and column loops (Figs. 14–16).

4.4. Modelling different scales

The next step was the validation of the CSTR model on different scale CCC instruments. Wood et al. [16] reported a scale up of ben-

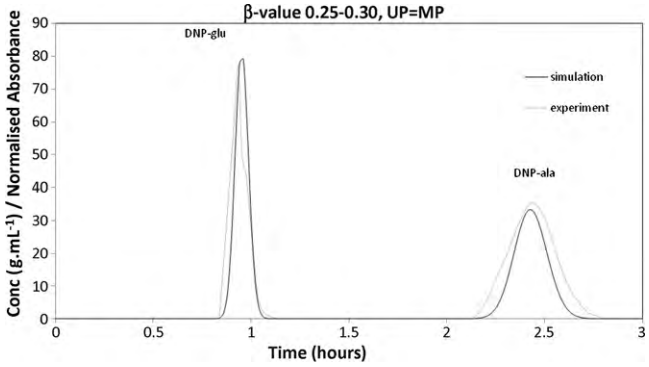

Fig. 13. Overlay of experimental results from Ref. [15] (Sandlin&Ito A) and modelling results; 750 mL column volume, 500 mL/h flow rate, upper phase as mobile phase, 65% stationary phase retention, β-value 0.25–0.30; 847 CSTRs in the model series.

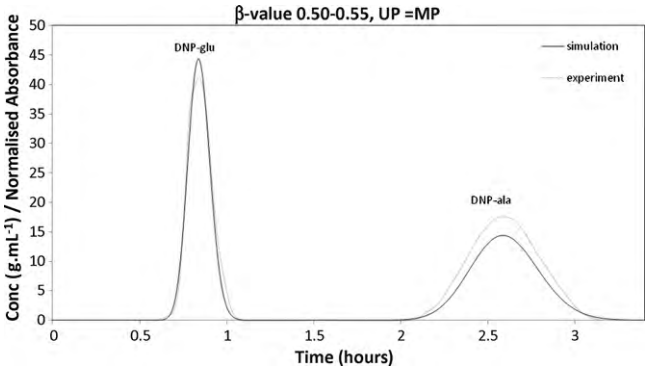

Fig. 14. Overlay of experimental results from Ref. [15] (Sandlin&Ito B) and modelling results; 750 mL column volume, 500 mL/h flow rate, upper phase as mobile phase, 79% stationary phase retention, β-value 0.50–0.55; 177 CSTRs in the model series.

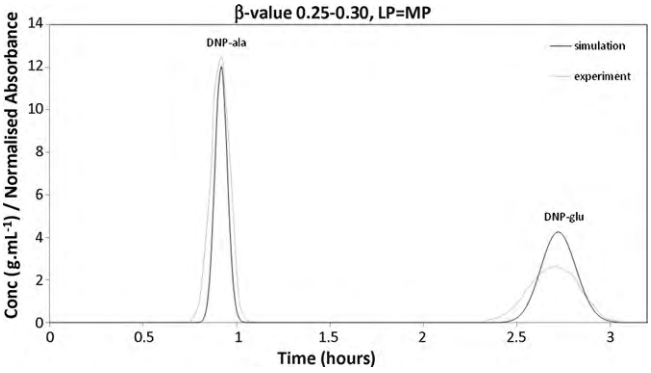

Fig. 15. Overlay of experimental results from Ref. [15] (Sandlin&Ito C) and modelling results; 750 mL column volume, 500 mL/h flow rate, lower phase as mobile phase, 84% stationary phase retention, β-value 0.25–0.30; 847 CSTRs in the model series.

zyl alcohol and p-cresol from an analytical scale column (DE Millie, 0.0054 L column volume) instrument to a production scale column (DE Maxi, 4.6 L column volume—see Section 3 for full description of experimental conditions). Sutherland et al. [17] later carried out a separation on another larger production scale column (DE Maxi New, 18 L column volume). These results were plotted and overlaid with simulated results that were produced using the described experimental conditions in Refs. [16,17].

The number of column loops was 51.5 for the DE Millie and with that the number of CSTRs was 132. The overlay of the experimental and modelling results of the analytical scale separation can be seen in Fig. 17. In this figure, the experimental results were pre-

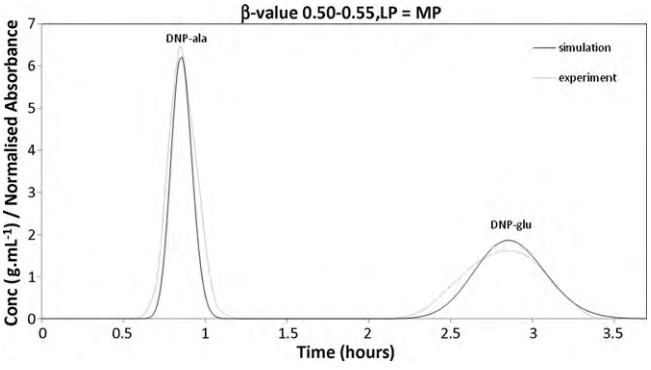

Fig. 16. Overlay of experimental results from Ref. [15] (Sandlin&Ito D) and modelling results; 750 mL column volume, 500 mL/h flow rate, lower phase as mobile phase, 87% stationary phase retention, β-value 0.50–0.55; 177 CSTRs in the model series.

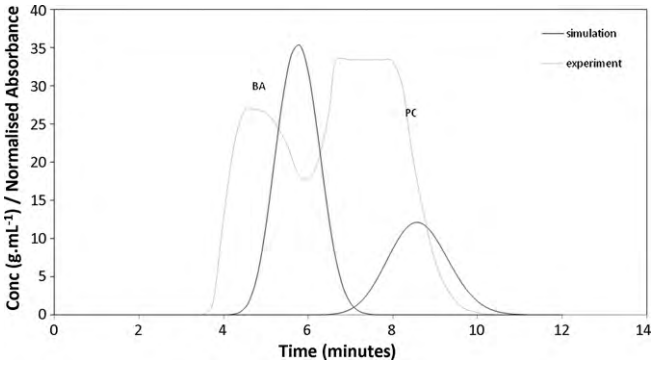

Fig. 17. Overlay of experimental results (dotted trace) from Ref. [16] (Wood et al. A) and modelling results (solid trace); 5.4 mL column volume, 1 mL min^{-1} mobile phase flow rate, lower phase as mobile phase, 64% stationary phase retention, β-value 0.69–0.74; 132 CSTRs in the model series.

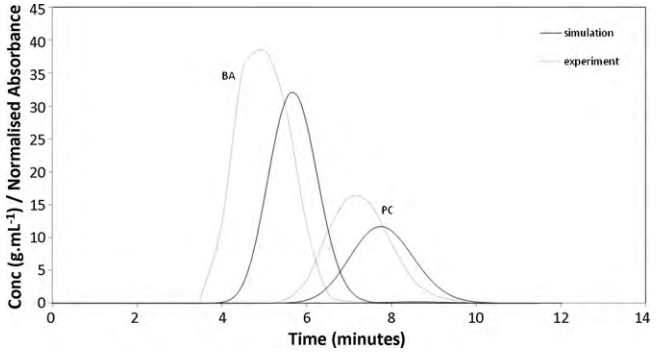

Fig. 18. Overlay of experimental results (dotted trace) from Ref. [16] (Wood et al. B) and modelling results; 4.6 L column volume, 850 mL min^{-1} mobile phase flow rate, lower phase as mobile phase, 47% stationary phase retention, β-value 0.69–0.74; 101 CSTRs in the model series.

sented in UV absorbance. It becomes apparent that p-cresol has a much higher molar absorption than benzyl alcohol, because the p-cresol peak is significantly taller despite having less than half of the benzyl alcohol's mass in the injected sample mixture. Since the model output is concentration rather than absorbance, the proportion of injected masses can be clearly seen in the peak areas of the simulation. The experimental and simulation resolutions were 0.69 [16] and 1.07, respectively. Since this experiment was an analytical scale experiment, the separation output was reported as UV absorption only. Due to the saturated absorbance of the p-cresol peak it is challenging to visually compare this chromatogram with the simulated chromatogram. However, the other experiments, which were carried out on production scale instruments, were presented as single solutes HPLC peak areas in respective fractions. This makes the comparison with simulated areas significantly easier.

Fig. 18 demonstrates an overlay of the first production scale result, which was produced with a DE Maxi, with the simulated results. The number of CSTRs in the series was 101. In this case the peak shapes compare better, because the experimental chromatogram was produced by plotting HPLC peak areas of respective fractions. Therefore, peaks in the experimental chromatogram are represented as individual traces of the two solutes rather than their combined absorbance in the overlapping area. By that, the experimental and model traces compare better than a UV monitoring of the column eluate, which was the case for the separation in Fig. 17 (Wood et al. A). Furthermore, the experimental and simulation resolutions were compared and gave 0.71 [16] and 0.74, respectively.

In Fig. 19 the experimental and simulated chromatograms were overlaid. The number of CSTRs for this simulation was 433. Here

Table 5
Resolutions of peaks obtained on three different lengths of instruments, R_S is the resolution obtained using the respective number of CSTRs, R_S^* is the resolution obtained using the previous column (half number of CSTRs) multiplied by $\sqrt{2}$.

n_{CSTRs}	Column volume (mL)	t_r peak 1 (min)	t_r peak 2 (min)	W peak 1 (min)	W peak 2 (min)	R_S	R_S^*	Error (%)
207	11	11.5	21.3	3.45	6.1	2.05	–	–
414	22	22.5	42.2	4.7	8.6	2.96	2.90	2.0
828	44	44.5	84	6.1	12.3	4.29	4.19	2.4

again the experimental chromatogram was created by plotting HPLC peak areas of respective fractions. In this experiment further stationary phase was displayed after sample injection. The stationary phase retention was 66% prior to injection, but only 31% at the end of the separation. In order to account for this change, the slope of the stationary phase retention for this separation was determined (66% stationary phase retention at solvent front to 31% at the end of the run). The stationary phase retention for each peak maximum was calculated by interpolation using this slope and was 60% for the benzyl alcohol peak and 43% for the p-cresol peak. The solutes were simulated individually with respective stationary phase retentions. The experimental resolution was 1.85 as stated in Ref. [17] and the simulation gave a resolution value of 1.48. However from the overlay of the chromatograms the peak shapes and resolutions look very similar and the peak resolution looks like just below 1.5 (a resolution greater than 1.5 gives baseline separation). Therefore the resolution value for the experimental result was recalculated from the chromatogram according to Eq. (18) and gave 1.43, which is very similar to the model output. The peak resolutions for the industrial scale instruments were precisely predicted and demonstrate the CSTR model's strength and robustness across different scales.

4.5. Effect of column length

Du et al. [18] established that by doubling the column length the resolution increased by a factor of $\sqrt{2}$. In order to test if the CSTR model conformed to this requirement, a separation with two solutes ($K_{D1} = 1$ and $K_{D2} = 2$) are simulated on three different columns. The respective column volumes were 11 mL, 22 mL, and 44 mL; whereas the column lengths doubled, the tubing bore was the same. This meant that the number of CSTRs in the series doubled, but the volume of the mixing zones did not change. Table 5 displays the solute retention times (t_r), the respective peak widths (W), the resolutions (R_S), the calculated resolutions (R_S^*), and the error in %. R_S^* of a column was calculated by multiplying the resolution for the smaller column with $\sqrt{2}$. The obtained error was very low and proves that the CSTR model complies with Du's [18] findings. In the CSTR model peak widths are primarily determined by the column length and the number of column loops (and with that the number of CSTRs), partition ratio, and the mixing zone (i.e. CSTR) volume. The last factor is comparable to the bead size in solid phase chromatography, which determines the efficiency of a separation. Hence it can be concluded that in a CCC experiment, if the partition ratio and the CSTR volume are the same, the peak widths depend on the column length.

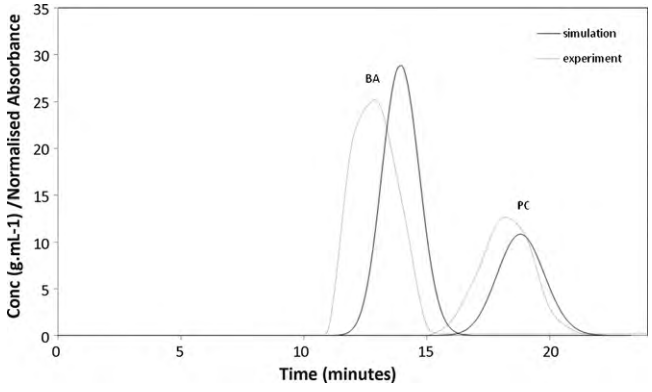

Fig. 19. Overlay of experimental results from Ref. [17] (Sutherland et al.) and modelling results; 18.0 L column volume, 850 mL min^{-1} mobile phase flow rate, lower phase as mobile phase, 66% stationary phase retention (only 31% left in the end of the separation), β-value 0.69–0.74; 124 CSTRs in the model series.

5. Conclusion

A novel CCC model was presented that can predict the elution profile of a column from scratch using instrument and operational parameters only. The model input was the column specifications such as column length, internal diameter, β-value, and number of column loops as well as the mobile phase flow rate, stationary phase retention, a solute's partition ratio, and its mass and volume. Using the instrument specifications the number and volume of CSTRs were calculated, which are specific for each column.

The CSTR model was validated using experimental results produced using a wide range of CCC instruments, which included early prototype columns, analytical, semi-preparative, and production scale instruments from various research laboratories. For the first time, it was possible to predict the elution profile of a CCC instrument from column dimensions and experimental settings, without resorting to empirical calibrations. Peak retentions as well as resolutions were predicted accurately for all separations.

This model does not only allow chromatograms to be predicted prior to carrying out a separation but can also help in building better performing CCC columns. Virtual separations can be produced when evaluating column dimensions, such as the column length and radius, number of loops, or β-value. This model provides valuable knowledge to optimise time and materials used in CCC operations, while contributing to establish CCC as a more generally applied chromatographic technique.

Nomenclature

c_{MP}	solute concentration in mobile phase (g L^{-1})
c_{SP}	solute concentration in stationary phase (g L^{-1})
CSTR	continuous-stirred tank reactor
d_c	column bore (m)
F	flow rate (L s^{-1})
i	increment
K_D	partition ratio
L_C	length of column (m)
L_{CSTR}	length of one CSTR (mixing zone) (m)
L_{Loop}	length of one loop (m)
n_{CSTRs}	number of CSTR in series
n_{Loop}	number of loops in column
P	pressure (N m^{-2})
R	orbital radius (m)
r_B	bobbin or planet radius (m)
r_C	column radius (m)

R_S	resolution
S_f	stationary phase retention
t	time (s)
t_E	elution time (s)
t_{inj}	injection time (s)
t_r	retention time of a solute (s)
V_C	column volume (L)
V_{CSTR}	volume of individual CSTR in series
V_{Loop}	volume of individual loop (L)
v_{mix}	mixing wave velocity ($m\,s^{-1}$)
V_{MP}	mobile phase volume (L)
v_{MP}	mobile phase velocity ($m\,s^{-1}$)
V_{Rt}	retention volume (L)
V_{SP}	stationary phase volume (L)
W_a or W_b	peak width of *a* or *b* (s)
β	ratio of planet radius to orbital radius
λ	detection wavelength (nm)

Acknowledgement

Financial grant is gratefully acknowledged from EC Marie Curie Actions (MRTN-CT-2006-036053 – InSolEx).

References

[1] Y. Ito, R.L. Bowman, Science 167 (1970) 281.
[2] Y. Ito, R.L. Bowman, J. Chromatogr. Sci. 8 (1970) 315.
[3] W.D. Conway, Countercurrent Chromatography: Apparatus, Theory and Applications, VCH, New York, 1990.
[4] P. Wood, L. Janaway, D. Hawes, I.A. Sutherland, J. Liq. Chromatogr. 26 (2003) 1373.
[5] Y. Ito, in: J. Cazes (Ed.), Encyclopaedia of Chromatography, Marcel Dekker, New York, 2001, p. 438.
[6] Y. Ito, J. Chromatogr. A 1065 (2005) 145.
[7] A.E. Kostanian, J. Chromatogr. A 973 (2002) 39.
[8] O. Levenspiel, Chemical Reaction Engineering, Wiley, New York, 1965.
[9] N.I. Gelperin, W.L. Pebalk, A.E. Kostanian, Flow Structure and Efficiency of Column Apparatus of Chemical Industry, Chimija, Moscow, 1977.
[10] A.M. Rozen, A.E. Kostanian, Proceedings of the 10th International Solvent Extraction Conference, ISEC-88, vol. 2, Moscow, 1988, p. 270.
[11] I.A. Sutherland, J. De Folter, P.L. Wood, J. Liq. Chromatogr. Relat. Technol. 26 (2003) 1449.
[12] J. de Folter, I.A. Sutherland, J. Chromatogr. A 1216 (2009) 4218.
[13] J.B. Friesen, G.F. Pauli, J. Liq. Chromatogr. 28 (2005) 2777.
[14] H. Guzlek, P.L. Wood, L. Janaway, J. Chromatogr. A 1216 (2009) 4181.
[15] J.L. Sandlin, Y. Ito, J. Liq. Chromatogr. 8 (1985) 2153.
[16] P. Wood, S. Ignatova, L. Janaway, D. Keay, D. Hawes, I. Garrard, I.A. Sutherland, J. Chromatogr. A 1151 (2007) 25.
[17] I. Sutherland, P. Hewitson, S. Ignatova, J. Chromatogr. A 1216 (2009) 4201.
[18] Q.Z. Du, C.Q. Ke, Y. Ito, J. Liq. Chromatogr. Relat. Technol. 21 (1998) 157.
[19] P.I. Barton, C.C. Pantelides, AIChE J. 40 (1994) 966.